Environmental Analysis of Warm-Season First Cloud-To-Ground Lightning Events over the Western Florida Peninsula

IVAN CHAVEZ,[a] SHAWN M. MILRAD,[a] DANIEL J. HALPERIN,[a] BRYAN MROCZKA,[b] AND KEVIN R. TYLE[c]

[a] *Meteorology Program, Applied Aviation Sciences Department, Embry-Riddle Aeronautical University, Daytona Beach, Florida*
[b] *National Weather Service Weather Forecast Office Tampa Bay Area, Ruskin, Florida*
[c] *Department of Atmospheric and Environmental Sciences, University at Albany, State University of New York, Albany, New York*

(Manuscript received 10 January 2022, in final form 2 July 2022)

ABSTRACT: Florida annually leads the United States in lightning-caused fatalities. While many studies have examined the lightning frequency maximum near Cape Canaveral, relatively little attention has been paid to the western Florida peninsula, which features a similar warm-season lightning event density. Of particular concern are first cloud-to-ground (FCG) lightning events in developing thunderstorms, which are difficult to predict with sufficient lead time and can catch people off guard. This study performs an environmental analysis of warm-season (May–September) FCG events (2014–21) across the western Florida peninsula using high-resolution model analysis data, including a comparison to null (No CG) days. FCG events and No CG days are first identified from ground-based lightning data and partitioned into nine synoptic-scale flow regimes. Next, spatiotemporal distributions of FCG events are elucidated for the western Florida peninsula. An ingredients-based analysis shows that the convective environment one hour before FCG events during strong south-southeast flow features the largest amounts of moisture, but the smallest instability values and weak midtropospheric lapse rates, primarily due to warm advection and moisture transport from the Atlantic Ocean. Environments one hour before FCG events in all nine flow regimes feature markedly greater instability values, larger relative humidity values, and steeper midtropospheric lapse rates than do No CG days. Results emphasize that instability and moisture are the key ingredients for warm-season FCG events in the region. Convective parameter statistical distributions and composite soundings populate an online dashboard that can be used by regional forecasters to better predict FCG events and increase alert lead times.

SIGNIFICANCE STATEMENT: Florida annually leads the United States in lightning fatalities. Of particular concern are first cloud-to-ground (FCG) lightning events, which are difficult to forecast and can catch people off guard especially during outdoor recreational activities and labor. We investigate the environmental characteristics of warm-season FCG events across the western Florida peninsula. Among nine regional flow patterns, some are associated with a less moist and more unstable atmosphere one hour before an FCG event, while other regimes exhibit a more moist and less unstable atmosphere. However, regardless of flow pattern, FCG events consistently feature substantially greater instability and moisture than do null events. Key findings are displayed on an online dashboard, to better inform regional forecasters.

KEYWORDS: Convection; Lightning; Sea breezes; Summer/warm season

1. Introduction

Primarily associated with warm-season sea-breeze processes, Florida experiences the largest number of mean thunderstorm days and annual lightning flash density of any state (e.g., Hodanish et al. 1997; Orville and Huffines 2001). Curran et al. (2000) produced a 35-yr (1959–94) U.S. lightning casualty climatology and reported Florida as having the most fatalities (345) and injuries (1178) of any state. During 1959–2019 (NWS 2021a), Florida (509 deaths) had more than twice the lightning-related fatalities of the next highest state (Texas, 231 deaths). Although annual lightning-related fatalities have decreased nationwide (NWS 2021a), Florida still regularly leads the United States each year. During the most recent decade (2010–19), Florida ranked first with 47 lightning-related fatalities and Texas was a distant second with 21 (NWS 2021a).

Research on thunderstorms and lightning in Florida is not new. Byers and Rodebush (1948) first noticed that thunderstorms occur 50% more frequently in the Florida peninsula than the panhandle, especially during the warm season. Lericos et al. (2002) assembled a synoptic climatology and found that the subtropical ridge position was key to warm-season thunderstorm location. Shafer and Fuelberg (2006, 2008) devised statistical procedures to help forecast warm-season lightning events, using environmental parameters and large-scale patterns. Rudlosky and Fuelberg (2011) found that warm-season flash density is considerably larger in central and southern Florida than in northern Florida, while the reverse is true during the cool season. Mazzetti and Fuelberg (2017) identified warm-season lightning flash rate maxima across central Florida, associated with the presence of multiple sea breezes, which result in a climatological surface convergence and ascent mechanism (e.g., Byers and Rodebush 1948; López and Holle 1986).

Lower-tropospheric sea-breeze convergence, in which the Atlantic and Gulf sea breezes meet each other and/or the

Mroczka's current affiliation: NOAA/Great Lakes Environmental Research Laboratory, Ann Arbor, Michigan.

Corresponding author: Shawn M. Milrad milrads@erau.edu

DOI: 10.1175/WAF-D-22-0005.1

prevailing wind, is the primary warm-season ascent mechanism for thunderstorms in the Florida peninsula (Byers and Rodebush 1948). Later observational (e.g., Gentry and Moore 1954; Estoque 1962; Kingsmill 1995) and numerical modeling (e.g., Pielke 1974; Dalu and Pielke 1989; Nicholls et al. 1991) studies added dynamical understanding to sea-breeze formation, convergence, and associated convection.

Central Florida, with its two sea breezes and multiple river and bay (e.g., Tampa Bay) breezes, is an ideal location to study warm-season lightning events and related convective environments. It is also home to two large metropolitan areas (Tampa Bay and Orlando), whose population increases over the past few decades have put millions more at risk of lightning-related casualties. According to U.S. Census Bureau data, the Tampa Bay metropolitan area had a population of 3.24 million in 2020, up from 2.79 million in 2010 (Statista 2021a), while the Orlando metropolitan area's 2020 population was 2.64 million, up from 2.14 million in 2010 (Statista 2021b). Most previous lightning research in the region has focused on the Cape Canaveral area, which is a regional lightning hotspot (e.g., Gremillion and Orville 1999; Rao and Fuelberg 2000; Hansen et al. 2010). However, west-central Florida including the Tampa Bay metropolitan area, has received considerably less research attention despite a similar lightning flash density to other regional hotspots (Lericos et al. 2002; Rudlosky and Fuelberg 2011).

In this study, we investigate warm-season first cloud-to-ground (hereafter FCG) lightning events across the western Florida peninsula, including but not limited to the National Weather Service Weather Forecast Office Tampa Bay's (hereafter NWS TBW) County Warning Area (CWA). FCG events are particularly important because of the considerable time people spend working outdoors (e.g., agriculture, construction) and in open outdoor spaces (e.g., beaches, golf courses, lakes), where they can be frequently caught off guard by developing thunderstorms. Improving awareness, forecasts, and alert lead times of FCG events are NWS TBW priorities. While a few radar-based (e.g., Mosier et al. 2011; Courtier et al. 2019) and satellite-based (e.g., *GOES-16* Day Cloud Phase; Elsenheimer and Gravelle 2019) algorithms have been tested to improve nowcasts of FCG events, much work remains to improve alert lead times. In addition, no previous study has completed an ingredients-based convective environment analysis (Doswell et al. 1996) of FCG events.

The primary objectives of this study are to:

- Establish an 8-yr climatology (2014–21) of warm-season (May–September) FCG events over the western Florida peninsula, using ground-based lightning network data.
- Partition FCG events into nine synoptic-scale flow regimes, already used operationally by NWS TBW.
- Perform a statistical and composite environmental analysis for FCG events within each flow regime, using high-resolution model analysis data. We particularly focus on moisture and instability, which are the two most important ingredients for Florida warm-season thunderstorms (e.g., Shafer and Fuelberg 2006, 2008).
- Compare FCG event environments to those of warm-season null events, elucidating key differences in convective ingredients.

The remainder of this paper is organized as follows: section 2 details data used and the convective environment analysis methodology. Section 3 presents results, including the spatial and temporal distributions of FCG events, statistical distributions of key convective environment parameters for FCG and null events, and composite soundings. Finally, section 4 provides a discussion, conclusions, and overview of potential future work.

2. Data and methods

a. Data

To identify FCG events, we used lightning data from the ground-based National Lightning Detection Network (NLDN; Orville 2008), which is owned and operated by Vaisala. NLDN accurately detects CG flashes, and its reliability has improved over time. Medici et al. (2017) found that NLDN detection efficiency improved from 65% to 80% in 1994 to greater than 95% following a 2013 network upgrade. For more details on the 2013 upgrade and associated improvements in detection efficiency, see Murphy et al. (2021). Koehler (2020) performed a 26-yr (1993–2018) CG flash density climatology using NLDN data and reported reliable results across the contiguous United States. Older 10-yr NLDN lightning climatologies include Orville and Huffines (2001) for the 1989–98 time period, and Holle et al. (2016) for 2005–14. To ensure that we only used NLDN data after the 2013 upgrade (Medici et al. 2017; Murphy et al. 2021), our study period covers the eight warm seasons (defined here as May–September) of 2014–21. Only CG flashes, as specified in NLDN data, were used to identify FCG events.

For the environmental analysis, we used the NOAA Rapid Refresh (RAP) model analysis (Benjamin et al. 2016). RAP covers the North American domain and was operationally implemented in 2012. It has a 1-h temporal resolution and 13-km grid spacing, with 51 vertical levels (Benjamin et al. 2016). The RAP has been used in several convective environment studies (e.g., Laflin 2013; Miller and Mote 2018).

b. Methods

An FCG event was defined as the first CG lightning occurrence on a given day of May–September 2014–21 within the black parallelogram shown in each panel of Fig. 1. This domain incorporates the western half of the Florida peninsula south of 29.5°N and was chosen so that we could identify all western Florida peninsula FCG events without being strictly limited to NWS CWA boundaries. However, the eastern half of the Florida peninsula was excluded because evaluating FCG events over the entire peninsula at once would result in an overwhelming majority of morning FCG events, given the sea/land breeze circulation that exists on each coast. We did, however, complete each aspect of our analysis presented here for the entire peninsular domain south of 29.5°N. For the sake of brevity, those results are not shown, but concise summaries are provided at various points throughout the text.

For our study domain (Fig. 1), we excluded FCG events over the Gulf of Mexico and Tampa Bay, to focus on potential lightning casualty events over land and smaller inland

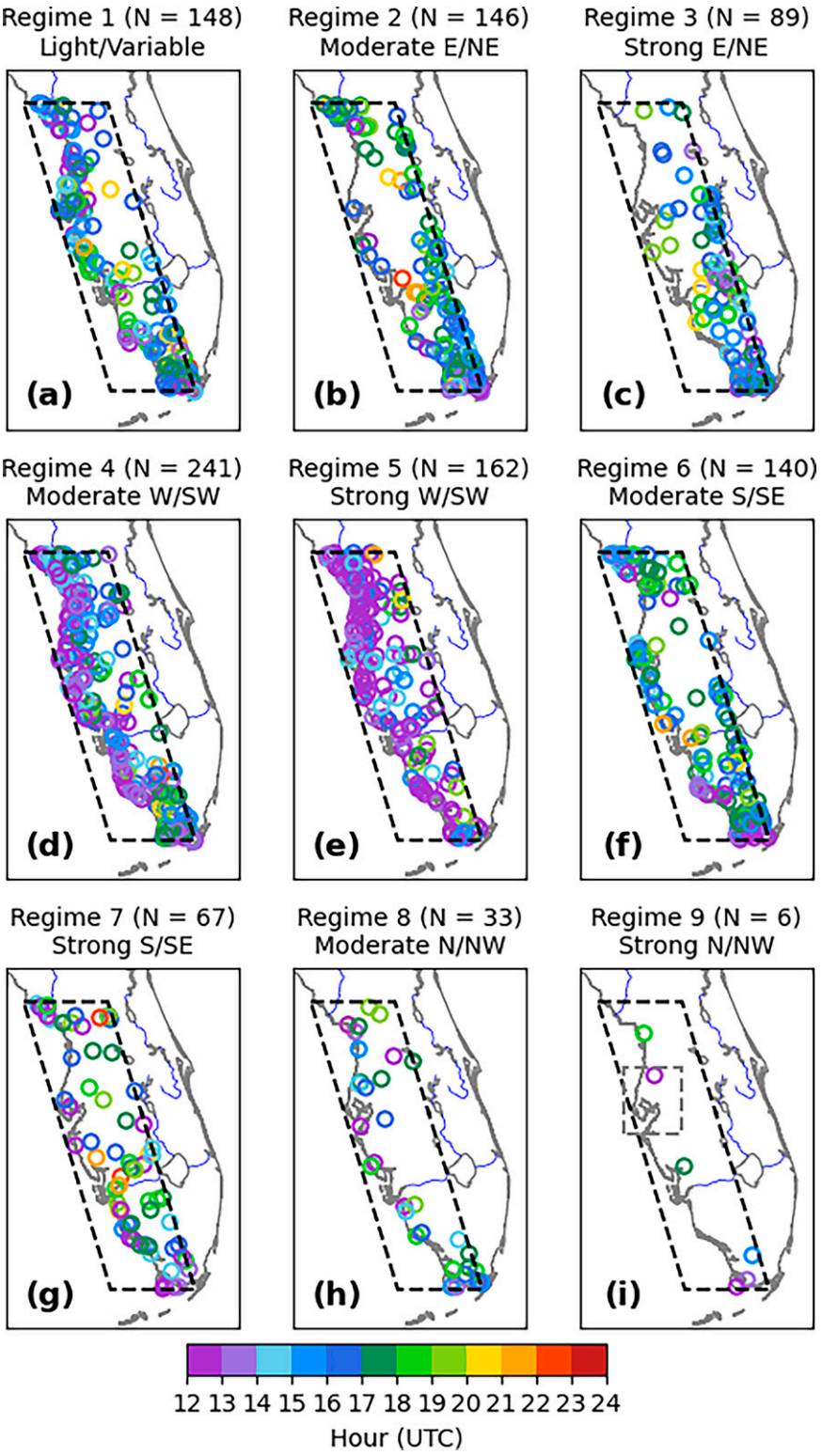

FIG. 1. For each flow regime, plots with open circles showing the time (UTC) of each FCG event based on NLDN lightning data within the study domain (black dashed parallelogram). (a)–(i) Regimes 1–9, respectively, with the number of FCG events (*N*) listed at the top of each panel. The small gray dashed box in (i) outlines the domain in which the flow regime is determined (Fig. 2).

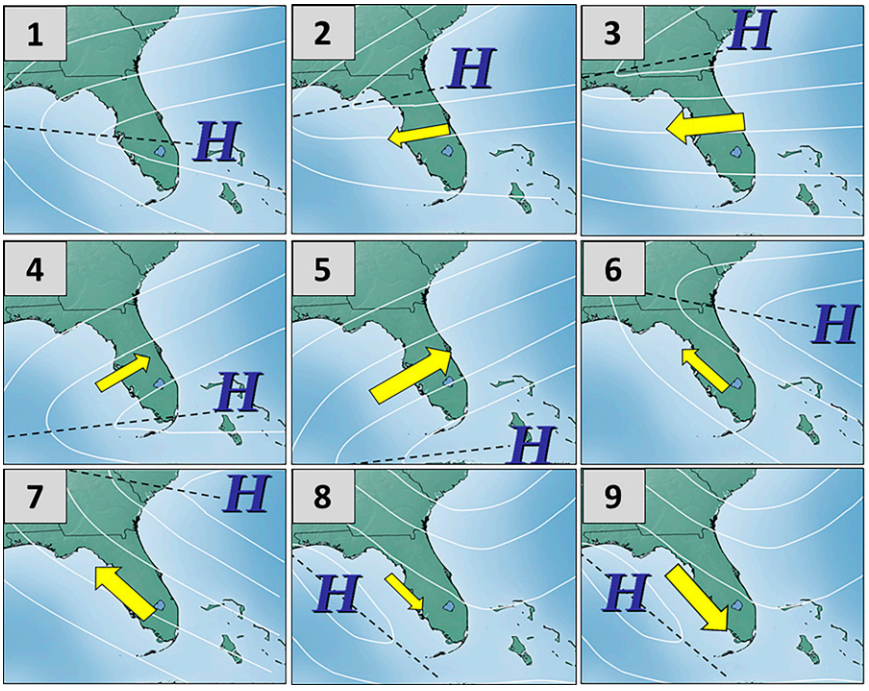

Regime #	Flow Direction	Flow Speed
1	Light/Var Any Direction	< 4 kt
2	E/NE 360° to 120°	4–10 kt
3	E/NE 360° to 120°	> 10 kt
4	W/SW 190° to 290°	4–10 kt
5	W/SW 190° to 290°	> 10 kt
6	S/SE 120° to 190°	4–10 kt
7	S/SE 120° to 190°	> 10 kt
8	N/NW 290° to 360°	4–10 kt
9	N/NW 290° to 360°	> 10 kt

FIG. 2. Schematic examples of and the specific criteria for the nine (numbered) synoptic-scale flow regimes analyzed in this study. The flow regime is determined for each day using the 1200 UTC RAP analysis 1000–700-hPa layer-mean vector wind within the gray dashed box in Fig. 1i. For each regime, yellow arrows represent the 1000–700-hPa layer-mean vector wind direction and magnitude, while the blue H letters represent the approximate locations of the climatological subtropical high pressure system located near Florida.

bodies of water. Furthermore, we only counted FCG events that occurred between 1200 and 2359 UTC. The 1200 UTC start time was chosen because the NWS TBW flow regimes used in this study (Fig. 2) were defined based on 1200 UTC 1000–700-hPa layer-mean vector wind. The 2359 UTC end time limits our study to daytime events, as local sunset is within 40 min of 0000 UTC during the entirety of the warm season (May–September). In addition, Fig. 3 shows that no FCG events in our study occurred after 2259 UTC, further justifying the use of our temporal boundary. Finally, using NOAA's historical hurricane tracks interface (NOAA 2021), we identified and removed nine total days on which a tropical cyclone center tracked within 250 km of our domain center. These nine days accounted for less than 1% of total FCG events (1032) in our climatology.

FCG events were partitioned into nine warm-season synoptic-scale flow regimes (NWS 2021b). The nine regimes were originally established by NWS TBW using 1200 UTC reanalysis data to calculate the 1000–700-hPa layer-mean vector wind near Tampa Bay. The 1000–700-hPa layer was chosen because it has the most direct interaction with the sea breeze (NWS 2021b). The area in which the 1200 UTC 1000–700-hPa layer-mean vector wind was calculated is shown by the gray box in Fig. 1i. Figure 2 shows the nine flow regimes, which also correspond to the position of the climatological warm-season subtropical high (blue H letters in Fig. 2) relative to Florida (e.g., Lericos et al. 2002; Shafer and Fuelberg 2006, 2008). All four wind direction sectors [east-northeast (E/NE), west-southwest (W/SW), south-southeast (S/SE), north-northwest (N/NW)] include a moderate [4–10 kt (1 kt ≈ 0.51 m s^{-1})] and strong (>10 kt) regime (Regimes 2–9; Fig. 2). Regime 1 (light/variable; Fig. 2) occurs when the 1200 UTC 1000–700-hPa layer-mean wind speed is <4 kt. NWS TBW has operationally used the flow regime partitioning scheme to forecast cloud cover, probability of precipitation (PoP), and quantitative precipitation during the warm season. Although reanalysis data were used for the original NWS TBW partitioning, we applied the scheme to 1200 UTC RAP data.

We investigated statistical distributions and composite means of the convective environments associated with FCG events for all flow regimes using RAP analysis data (sections 3b and 3c). Statistical distributions and composite means were produced for one (−1 h), two (−2 h), and three (−3 h) hours prior to FCG events. The RAP hourly analysis time immediately prior to each FCG event was defined as 0 h. For example, if a FCG event occurred at 1846 UTC, the 0- and −1-h RAP analysis times would be 1800 and 1700 UTC, respectively. The results in sections 3b and 3c do not focus on 0 h because one of our primary objectives is to improve alert lead times of FCG events. As 0 h could potentially be as little as one minute before an event (e.g., 1800 UTC RAP analysis for an 1801 UTC FCG event), analyses of slightly earlier times will provide forecasters more useful information. Convective parameter distributions and composite means did not differ much between −1, −2, and −3 h, and as such we only show −1-h results.

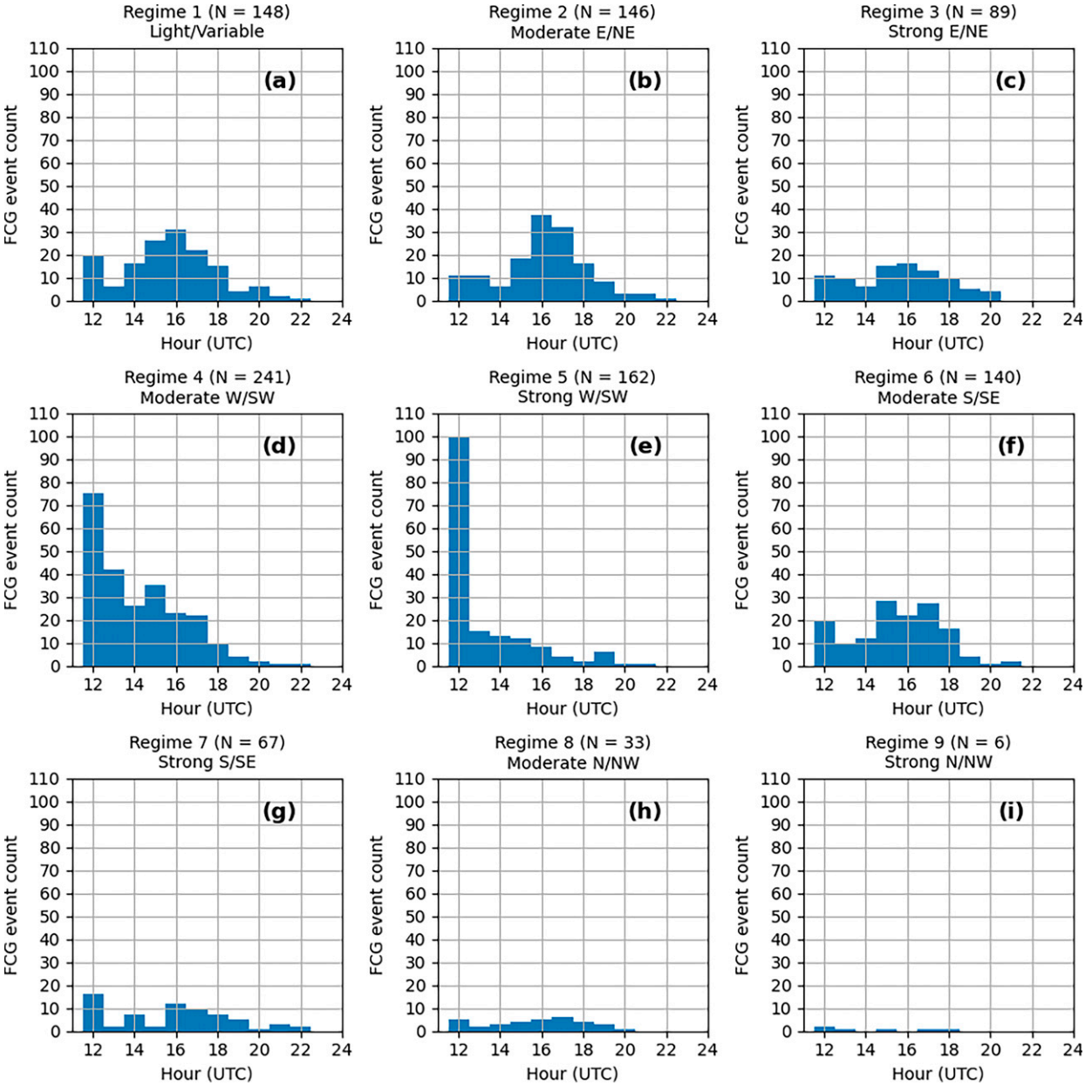

FIG. 3. For each synoptic-scale flow regime (Fig. 2), histograms showing the temporal distributions (UTC) of FCG events. The total number of FCG events in each regime (N) is listed at the top of each panel.

We also investigated parameter distributions on days when no FCG events occurred (hereafter No CG days). The parameter distributions of No CG days are shown for 1200 and 1800 UTC, to compare and contrast between FCG and No CG convective environments (section 3b). For FCG events, the environmental variable values shown in the box-and-whisker plots in section 3b were taken from the RAP analysis grid point closest to each FCG event on a given day. On No CG days, environmental parameter values were taken from an areally averaged 3×3 grid box at the center (27.3°N, 81.975°W) of our study domain (Fig. 1). The composite soundings described in section 3c were constructed using composite mean values within each flow regime, including mean surface temperature and dewpoint to calculate the parcel path and associated convective indices. We compared a small subset of RAP analysis soundings to observed TBW radiosonde soundings and they were quite similar. However, to help quantify uncertainty that can be smoothed out in composite means, our soundings also include the environmental temperature and dewpoint for the 25th and 75th percentiles within the FCG event and No CG day distributions (section 3c). The 25th and 75th percentiles were chosen to correspond with the interquartile ranges (boxes) shown in the box-and-whisker plots in section 3b.

3. Results

a. Spatiotemporal distributions of daily FCG events

The spatiotemporal distributions of FCG events (2014–21), as well as the number of events within each regime, are shown in Fig. 1. In addition, histograms depicting the temporal distributions of FCG events are shown in Fig. 3. Regimes 1, 4, and 5 (Figs. 1a,d,e) feature the most (148, 241, and 162, respectively) FCG events in our study. Regime 1 (light/variable) events are relatively evenly distributed throughout the day but exhibit a frequency peak in the early afternoon (Fig. 3a). Particularly in the southern half of our domain, many Regime 1 afternoon (1600–2200 UTC) FCG events are located in the eastern portion of the domain (Fig. 1a), where the Gulf and Atlantic sea breezes frequently interact on weak background flow days (e.g., Byers and Rodebush 1948; Estoque 1962). Meanwhile, the vast majority of Regime 4 and 5 (W/SW flow) events occur during the morning (1200–1600 UTC) hours (Figs. 3d,e), largely near the Gulf Coast (Figs. 1d,e). These morning FCG events are likely related to the remnant nocturnal land-breeze circulation (e.g., Estoque 1962) interacting with the W/SW background flow. In Regimes 4 and 5, afternoon events predominantly occur in the eastern part of our domain (Figs. 1d,e), as W/SW background flow interacts with the Atlantic sea breeze. These regimes would likely pose the largest afternoon thunderstorm threat to the eastern Florida peninsula (not shown), as individual thunderstorms drift eastward and new storms form later in the day.

In Regimes 2 and 3 (E/NE flow), most FCG events occur in the eastern part of the study domain (Figs. 1b,c), as thunderstorms from the eastern Florida peninsula drift westward during the late morning and early afternoon (not shown). This is exemplified by the temporal distributions (Figs. 3b,c), which show frequency peaks in the early to midafternoon. Both regimes exhibit a secondary late-afternoon cluster in southwestern Florida near Fort Myers and Naples (Figs. 1b,c). This cluster is likely related to interaction with the Gulf sea breeze in southwestern Florida as the E/NE background flow crosses the state, particularly in strong events (Regime 3; Fig. 3c).

Regimes 6 and 7 (S/SE flow) and 8 and 9 (N/NW flow) (Figs. 1f–i) feature fewer FCG events than the E/NE (2 and 3) and W/SW flow regimes (4 and 5). Regimes 6–9 also exhibit few morning FCG events (Figs. 3f–i), especially near the Gulf Coast (Figs. 1f–i). The most common time for FCG events in all four regimes is early to midafternoon (Figs. 3f–i). In Regime 6 (moderate S/SE; Fig. 1f), the majority of afternoon FCG events occur in the southern half of the study domain, where the S/SE background flow interacts with the Gulf sea breeze. Regime 7 (strong S/SE flow; Fig. 1g) is similar to Regime 6, albeit with less than half the number of events. Finally, in Regimes 8 and 9 (N/NW flow; Figs. 1g,h), there are only 33 and 6 total events, respectively, with most occurring in the early afternoon (Figs. 3h,i). Regime 8 (moderate N/NW flow) exhibits a cluster of afternoon events in the southeast corner of the study domain (Fig. 1h), where the background flow interacts with the Atlantic sea breeze.

The biggest differences in spatiotemporal distributions between our domain and the entire peninsular domain (not shown) occur in flow regimes with an easterly component [Regimes 2 and 3 (E/NE) and Regimes 6 and 7 (S/SE)]. In those regimes, the overwhelming majority of FCG events in the full peninsular domain occur between 1200 and 1400 UTC on the east and southeast coasts of Florida (not shown). This emphasizes that the first thunderstorms on any given day typically occur in the portion of the Florida peninsula where the synoptic-scale flow originates (e.g., southeast Florida for S/SE flow regimes). However, within those flow regimes, stronger storms typically occur in the western Florida peninsula later in the day. Therefore, we believe our choice of domain focused on the western half of the Florida peninsula is justified.

b. Convective parameter distributions

The necessary ingredients for moist convection are lift, moisture, and instability (Doswell et al. 1996), with vertical wind shear as a fourth ingredient that can increase thunderstorm duration and severity. During the warm season, vertical wind shear is often weak over the Florida peninsula, barring a tropical cyclone or unseasonably strong midlatitude trough (e.g., Schwartz and Bosart 1979; Rudlosky and Fuelberg 2011). Furthermore, excluding tropical cyclones, ascent is typically forced by sea-breeze interactions and/or surface heating (e.g., Blanchard and Lopez 1985; Milrad and Herbster 2017). Since we eliminated tropical cyclone days from our climatology (section 2b), we primarily focus on variables that assess moisture and instability, given the weak synoptic-scale lift and vertical shear in the Florida peninsula during the warm season.

Figure 4 shows box-and-whisker plots of surface-based CAPE (SBCAPE) at −1 h for FCG events, and at 1200 and 1800 UTC for No CG days. In FCG events, all regimes have median and mean SBCAPE values between 2000 and 3000 J kg^{-1}, with the smallest median and mean SBCAPE values observed in Regimes 5 (Fig. 4e) and 7 (Fig. 4g), respectively. Regime 5 events occur overwhelmingly around 1200 UTC (Figs. 1e,3e). Meanwhile, Regime 7 events are typically associated with high PoPs throughout west-central and southwestern Florida due to moisture advection by southeasterly winds from the Atlantic Ocean (NWS 2021b). In contrast, Regime 6 has the largest mean and median SBCAPE values (Fig. 4f), with both exceeding 2500 J kg^{-1}. Therefore, the smallest and largest mean SBCAPE values occur in two regimes that have the same flow direction (Regimes 6 and 7; S/SE), but different flow intensities. Throughout all FCG event regimes, SBCAPE at −1 h has a large range, with some individual events having SBCAPE values near 0 J kg^{-1} (e.g., Fig. 4d) and others with values > 4000 J kg^{-1} (e.g., Figs. 4d–f). Nevertheless, the large majority of FCG events (i.e., the three highest quartiles) in all regimes occur with SBCAPE values > 1500 J kg^{-1}, a potentially important benchmark for forecasters.

Overall, our SBCAPE results (Fig. 4) mirror those of Livingston et al. (1996), who found that large CAPE values were strongly correlated (>0.5) with summer CG lightning activity over Georgia. The dramatic SBCAPE differences between FCG and No CG days in all regimes reinforce this point (Fig. 4). Although No CG mean and median 1800 UTC SBCAPE values are generally larger than 1200 UTC values (Fig. 4), both pale in

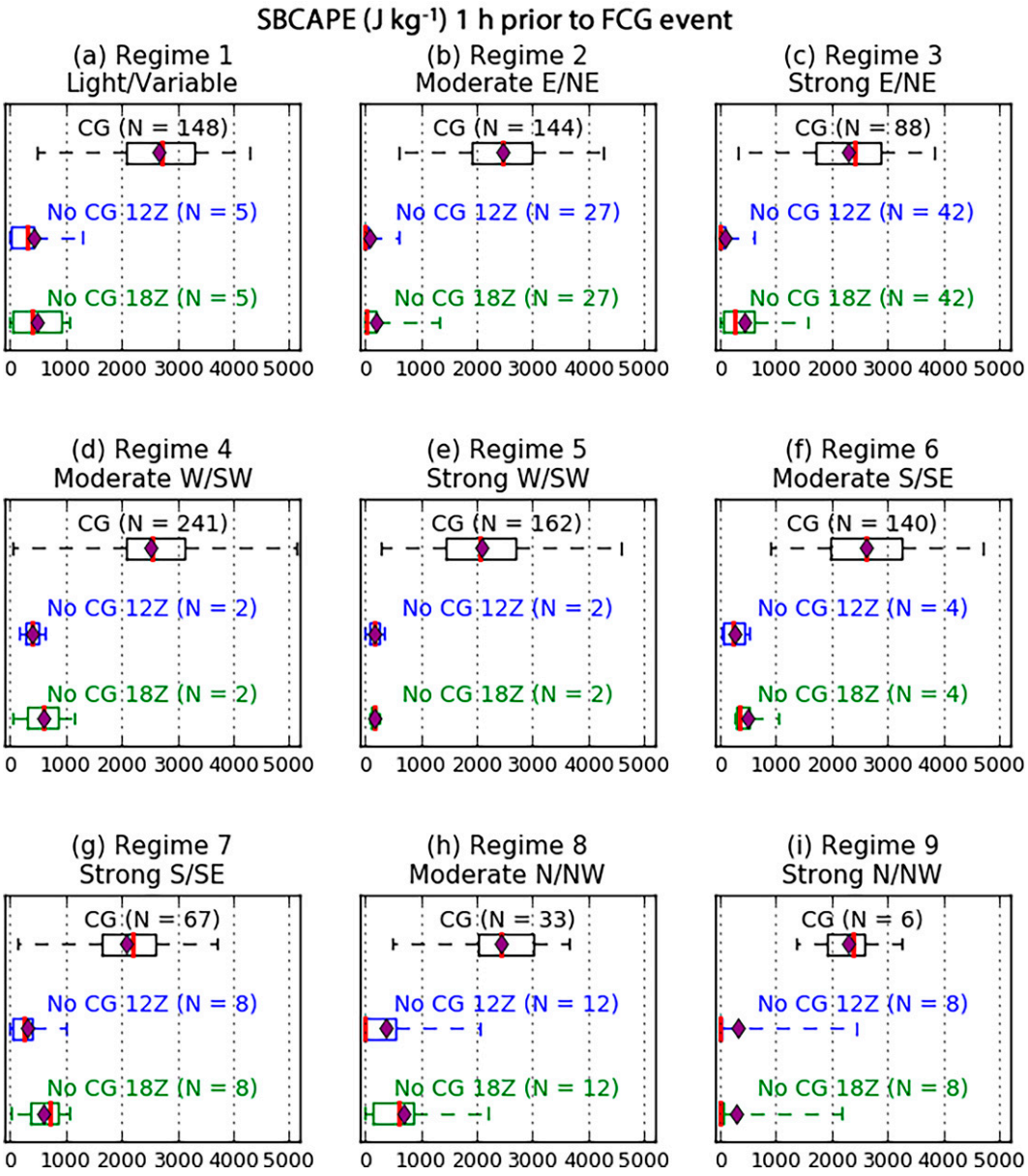

FIG. 4. Box-and-whisker plots showing the distribution of RAP analysis surface-based CAPE (SBCAPE; J kg^{-1}) 1 h prior (−1 h) to FCG events (black) at the RAP grid point closest to each FCG event, and 1200 UTC (blue) and 1800 UTC (green) for No CG days using the area average of a 3 × 3 grid box at the center (27.3°N, 81.975°W) of our study domain (Fig. 1). (a)–(i) Flow regimes 1–9, respectively. Median and mean values are marked by a red line and purple diamond, respectively. Box edges represent the 25th and 75th percentile values in the distribution, with the box representing the interquartile range. Whiskers represent the minimum and maximum values in the distribution. The number of events (*N*) in each regime is shown above each box-and-whisker plot.

comparison to SBCAPE at −1 h in FCG events, emphasizing the importance of buoyant instability to warm-season Florida thunderstorms. Finally, we emphasize that the results shown in Fig. 4 for our study domain are very similar to those for the full peninsular domain (not shown), supporting the robustness of our methodology.

SBCAPE in the hail-growth-zone (HGZ), with the HGZ defined as the −10° to −30°C layer (e.g., Foote 1984; Knight and Knight 2001), has been primarily used to improve forecasts of hail size (e.g., Blair et al. 2011; Johnson and Sugden 2014). Some studies (e.g., Kalina et al. 2016) have found HGZ SBCAPE to be inversely related to thunderstorm intensity and hail size, because lightning rates decrease during wet hail growth (Rudlosky and Fuelberg 2013). While investigating severe thunderstorms in east-central Florida, Williams et al. (1999) postulated that severe hail formation may lag

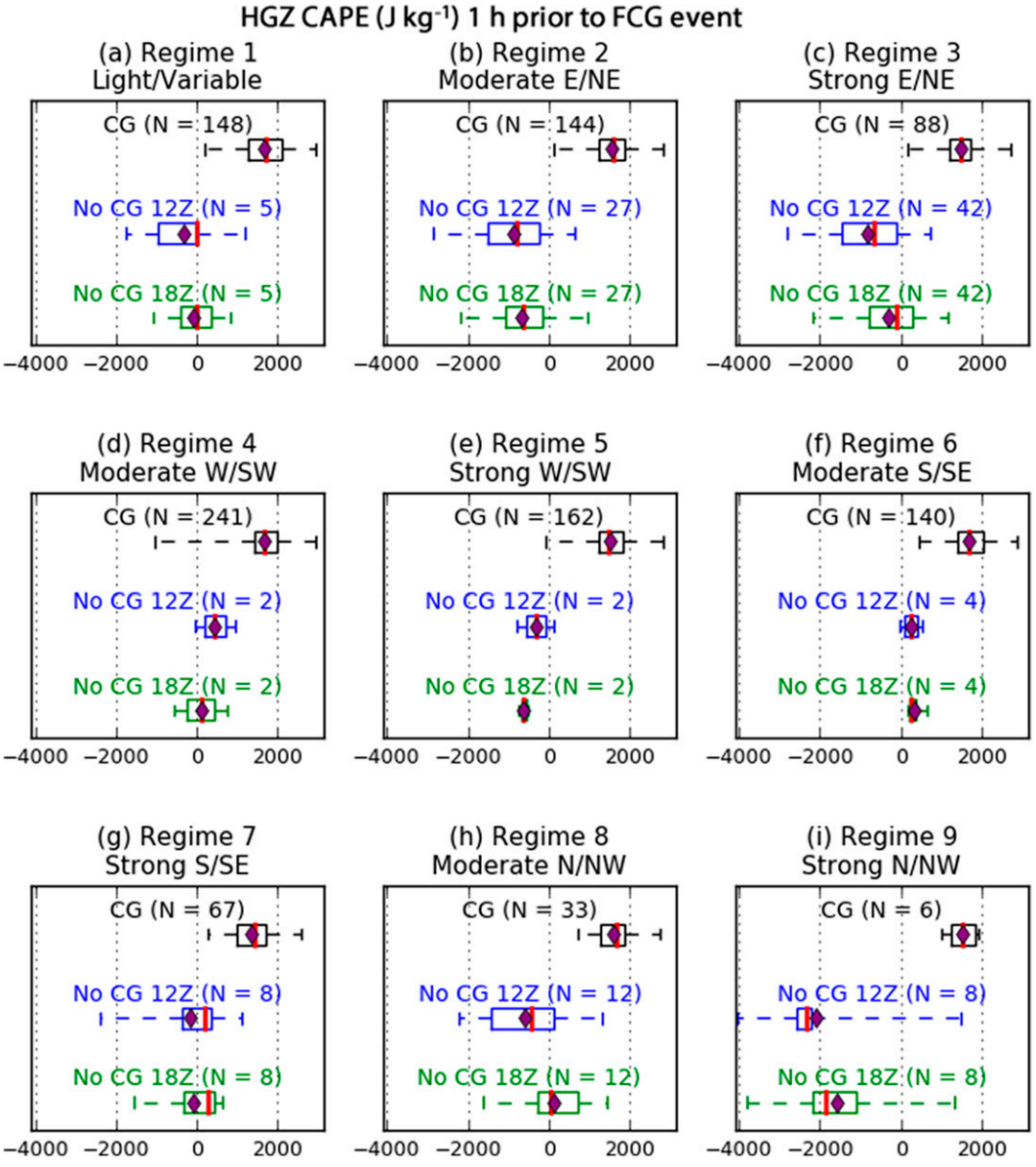

FIG. 5. As in Fig. 4, but for SBCAPE (J kg^{-1}) in the hail growth zone (HGZ), defined here as the pressure layer where the temperature is between −10° and −30°C. Because RAP analysis data has vertical levels only every 25 hPa, our definition of the HGZ may not capture the true −10° to −30°C layer in its entirety.

lightning flash rate increases by 10–20 min. To our knowledge, no previous study has investigated the use of HGZ SBCAPE and/or the height of the −10°C surface (bottom of the HGZ) as potential discriminators for FCG events.

Figure 5 shows HGZ SBCAPE for FCG (−1 h) and No CG days. As for SBCAPE (Fig. 4), Regimes 5 and 7 feature the smallest median and mean HGZ SBCAPE values, respectively, for FCG events (Figs. 5e,g). Regime 7 events have the weakest midtropospheric environmental lapse rates (section 3c), which correspond to smaller HGZ SBCAPE values. For FCG events, all regimes have median and mean HGZ SBCAPE values between 1000 and 2000 J kg^{-1}. Furthermore, FCG events in all regimes exhibit substantially larger HGZ SBCAPE than No CG days. To that end, the 1200 and 1800 UTC mean and median HGZ SBCAPE values are negative in at least six and four No CG day regimes, respectively. As with the SBCAPE results in Fig. 4, these findings emphasize how important buoyant instability is to warm-season Florida thunderstorms. Finally, as for SBCAPE, the results shown in Fig. 5 for our study domain are extremely similar to those for the full peninsular domain (not shown).

We next explore distributions of the −10°C height surface, the bottom of the HGZ and a potential predictor of thunderstorm intensification (e.g., Rudlosky and Fuelberg 2013).

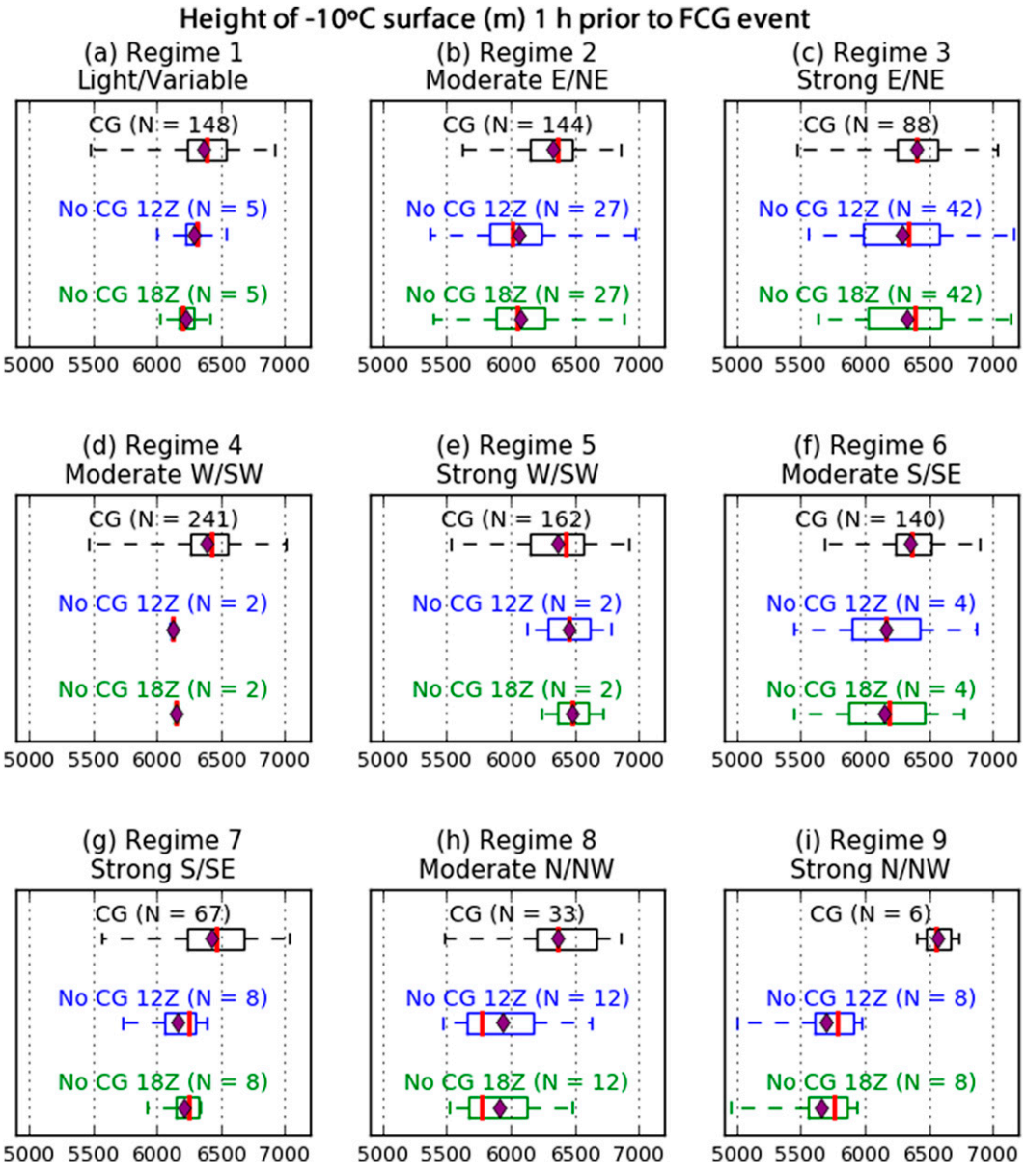

FIG. 6. As in Fig. 4, but for the height (m) of the −10°C surface, the bottom of the HGZ.

Figure 6 shows that all FCG event regimes have median and mean −10°C heights in the 6000–6500-m range, except Regime 9 (Fig. 6i) which has only six total FCG events. All regimes except Regime 9 exhibit a fairly wide range of heights, but relatively small interquartile ranges (Fig. 6). The median and mean −10°C heights are lower for No CG days (compared to FCG events) in all regimes except Regime 5, which had only two No CG days (Fig. 6). However, unlike SBCAPE and HGZ SBCAPE, most regimes do not exhibit substantial differences between FCG and No CG days (at either 1200 or 1800 UTC). The exceptions are Regimes 8 and 9 (N/NW), which have a median −10°C height more than 500 m lower on No CG days. Finally, we emphasize that results for our domain were extremely similar to those for the entire peninsula (not shown).

Precipitable water (PWAT) indicates the amount of water vapor within the troposphere and can help diagnose the moisture ingredient necessary for moist convection (Doswell et al. 1996). In studies of warm-season convection in Canada and India, respectively, Burrows et al. (2005) and Madhulatha et al. (2013) found PWAT to be one of the most skillful predictors of lightning frequency. More recently, Gijben (2016) found PWAT to be an excellent predictor of lightning occurrences in South Africa, as there were statistically significant PWAT differences between lightning and nonlightning days.

Figure 7 shows that for FCG events at −1 h, all regimes have median and mean values between 45 and 55 mm (50.8 mm = 2 in.), emphasizing the importance of large PWAT to warm-season Florida thunderstorms (e.g., Shafer and Fuelberg 2006, 2008)

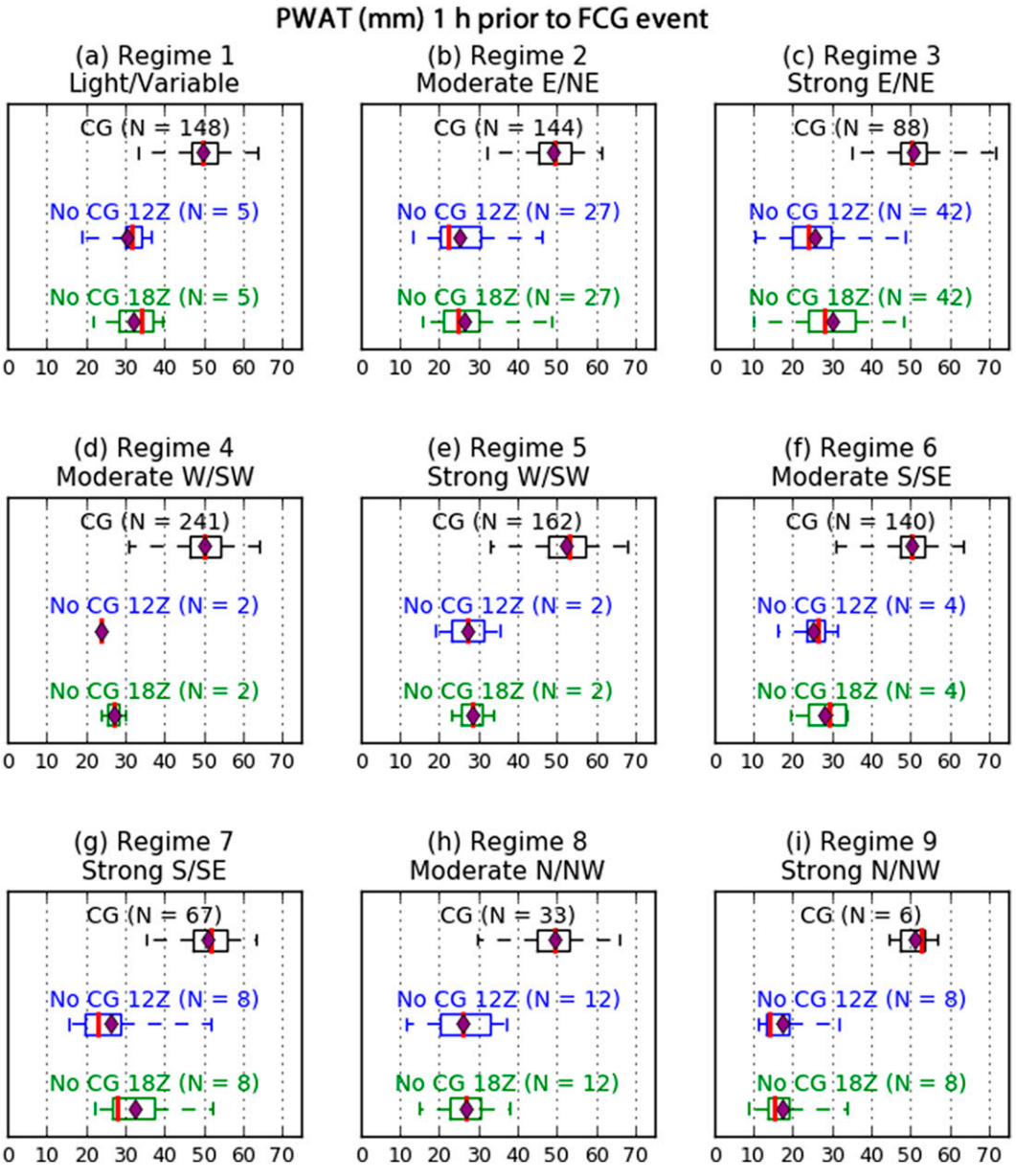

FIG. 7. As in Fig. 4, but for precipitable water (PWAT; mm).

and potentially serving as a useful benchmark for regional forecasters. The largest median and mean values are observed in Regimes 5 (Fig. 7e), 7 (Fig. 7g), and 9 (Fig. 7i), although overall there are not large differences among the nine regimes. For FCG events, Regime 7 is characterized by large values of PWAT and relatively small SBCAPE values (Fig. 4g), as the S/SE flow advects moisture from the Atlantic and Caribbean toward the western Florida peninsula. On the other hand, Regime 3 FCG events are characterized by relatively large values of both SBCAPE (Fig. 4c) and PWAT (median/mean values $>$ 50 mm; Fig. 7c). For regimes in which the background flow enters the study domain from the land (E/NE and S/SE flow), strong background flow (Figs. 7c,g) features larger median/mean PWAT than does moderate flow (Figs. 7b,f). This suggests that when the synoptic-scale flow comes from a drier (i.e., land) source region, stronger background winds are required to transport larger PWAT into the study domain from the Atlantic Ocean and Caribbean.

PWAT differences between FCG and No CG days are substantial across all regimes (Fig. 7). Median differences between FCG and 1800 UTC No CG days exceed 20 mm in seven of nine regimes, with Regimes 8 and 9 exhibiting median differences of approximately 25 and 30 mm, respectively (Figs. 7h,i). This suggests that large values of PWAT are necessary for FCG events. The largest differences in PWAT between FCG and No CG days occur in regimes with

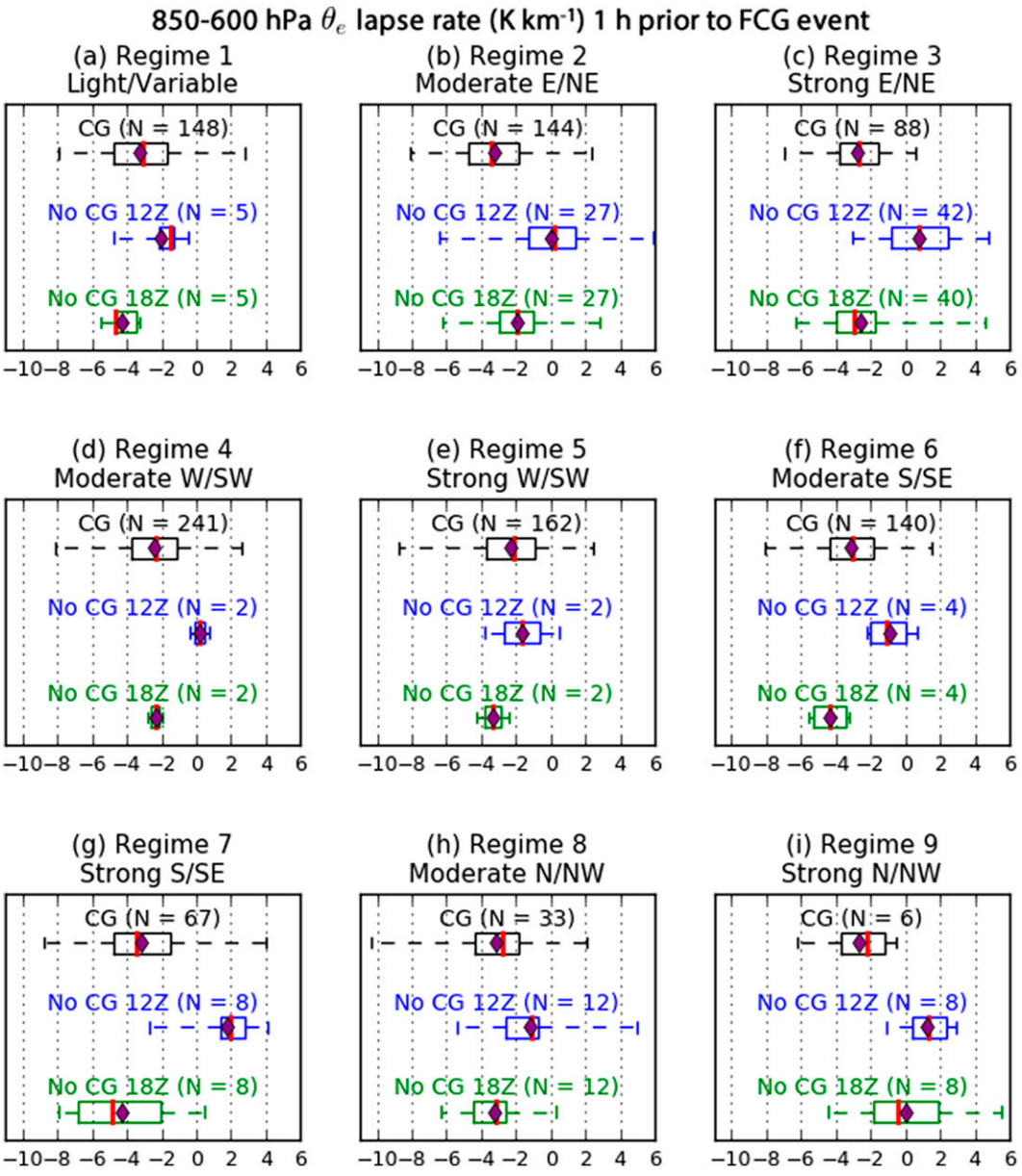

FIG. 8. As in Fig. 4, but for 850–600-hPa equivalent potential temperature (θ_e) lapse rate (K km^{-1}).

typically drier background flow (i.e., the N/NW Regimes 8 and 9), while smaller differences are observed in regimes where the flow is typically associated with more humid air (i.e., the S/SE Regimes 6 and 7). To that end, the mean PWAT difference in Regime 7 between FCG and 1800 UTC No CG days is less than 20 mm (Fig. 7g). Finally, as with the convective ingredients explored earlier, results for the full peninsula domain (not shown) were similar to those presented here.

Some previous research has indicated that equivalent potential temperature (θ_e) can be a useful predictor of lightning activity (e.g., Williams et al. 2005). In examining lightning days in Georgia, Livingston et al. (1996) found a moderate (~0.4) positive correlation between 850-hPa θ_e values and CG activity. More recently, for India and South Africa, respectively, Madhulatha et al. (2013) and Gijben (2016) found that θ_e lapse rates could be a useful predictor of lightning activity because they measure the amount of convective (potential) instability in the lower to midtroposphere.

Figure 8 shows 850–600-hPa θ_e lapse rates, similar to the layers chosen by Madhulatha et al. (2013) and Gijben (2016). We tried other midtropospheric layers (e.g., 850–500 hPa) and results were similar (not shown). Convective (potential) instability is defined as $d\theta_e/dz < 0$ (Schultz and Schumacher 1999). All FCG event regimes feature 850–600-hPa convective instability (Fig. 8), which is not surprising given that every

FCG event is associated with at least one thunderstorm. However, there are some key differences among regimes. Based on median and mean values for FCG events, Regime 5 (Fig. 8e) features the least convectively unstable environment. In contrast, Regime 8 (Fig. 8h) exhibits among the most convectively unstable median and mean environments, although many other regimes (e.g., Regime 1) have similar values. Although convective instability is a measure of layer stability, results for Regimes 5 and 8 correspond to our SBCAPE (buoyant parcel instability) results (Figs. 4e,h), in which Regime 5 has the smallest median SBCAPE value and Regime 8 has one of the largest. Interestingly, Regime 7 has the smallest mean SBCAPE value (Fig. 4g) but is more convectively unstable than most other regimes (Fig. 8g), suggesting that Regime 7 events may be preferentially associated with convective instability as opposed to buoyant instability.

For all regimes, FCG events are more convectively unstable than No CG days at 1200 UTC (Fig. 8). However, the same is not true at 1800 UTC in No CG days. In seven of the nine regimes (Fig. 8), FCG events have similar or less convective instability than 1800 UTC No CG days (Fig. 8). We caution, however, that several regimes have very few No CG days. Only in Regimes 2 and 9 do FCG events exhibit substantially greater convective instability than 1800 UTC No CG days. This suggests larger midtropospheric lapse rates in these events compared to null events. We expand on these attributes further using composite soundings in the next section. Finally, as with all convective ingredients explored to this point, results for the peninsular domain (not shown) were very similar to the domain shown in this paper.

c. *Composite soundings*

Figures 9 and 10 show composite RAP soundings at −1 h for FCG events and 1800 UTC for No CG days, respectively. The parcel paths in Figs. 9 and 10 were calculated using the composite mean 1000-hPa temperature and dewpoint in each regime. This differs from the statistical distributions shown in Figs. 4–8, in which convective parameters were calculated individually for each case. Therefore, the composite mean parameter values written on the panels in Figs. 9 and 10 differ slightly from those in Figs. 4–8. To elucidate how representative of individual events the composite mean soundings are, we also include 25th and 75th percentile environmental temperatures and dewpoints (dashed red and green lines, respectively) in Figs. 9 and 10.

For the FCG event composites (Fig. 9), there are substantial similarities among the nine regimes, as well as important subtle differences. Simplistic convective indices such as the K index (KI) and lifted index (LI) are quite similar among all nine regimes, which is not surprising since all FCG events are associated with thunderstorms. The three largest composite mean SBCAPE values are observed in Regimes 1, 4, and 6 (Figs. 9a,d,f), while the three smallest values are in Regimes 3, 7, and 9 (Figs. 9c,g,i). Intriguingly, the largest (Regime 6) and smallest (Regime 7) regimes have the same synoptic-scale flow direction (S/SE). However, moderate S/SE (Regime 6) events have an SBCAPE that is approximately 500 J kg^{-1} larger than strong S/SE (Regime 7) events. The key difference appears to be much steeper midtropospheric environmental lapse rates in Regime 6 (Fig. 9f) compared to Regime 7 (Fig. 9g). This may in part be caused by weak warm advection in Regime 7, as demonstrated by the slightly veering wind profile with height (Fig. 9g). Warm advection increases temperatures in the midtroposphere, thereby reducing environmental lapse rates.

For FCG events, Regimes 5 and 7 (Figs. 9e,g) have the largest composite mean PWAT values, while Regimes 2 and 8 have the smallest (Figs. 9b,h). This matches our findings in Fig. 7 (section 3b) and suggests that strong W/SW (Regime 5) and S/SE (Regime 7) background flow both transport higher moisture values toward the study domain, from the Gulf of Mexico and Atlantic Ocean/Caribbean, respectively. In contrast, moderate E/NE (Regime 2) and N/NW (Regime 8) flow result in a slightly drier troposphere.

A recurring theme throughout all FCG event composite soundings is that the 25th and 75th percentile environmental temperature profiles are quite similar, but the 25th and 75th percentile environmental dewpoint profiles are not, particularly in the midtroposphere (Fig. 9). This suggests that FCG events in each regime have similar midtropospheric environmental temperature lapse rates and that each composite mean temperature profile represents most cases within that regime. However, FCG events in all regimes occur across a wide range of midtropospheric environmental dewpoint lapse rates, suggesting that midtropospheric saturation is not required for FCG events.

Although there are important composite sounding differences among FCG event regimes, those differences pale in comparison to the differences between FCG (Fig. 9) and 1800 UTC No CG (Fig. 10) composite soundings in all regimes. Among other things, 1800 UTC No CG days exhibit substantially smaller values of surface and midtropospheric relative humidity, SBCAPE, and PWAT. Only three regimes in 1800 UTC No CG days have SBCAPE > 0 J kg^{-1}, and PWAT values are generally 20–25 mm less (Fig. 10) than the corresponding values in FCG events (Fig. 9). These results emphasize the importance of moisture and instability to warm-season Florida thunderstorms. Even the Regime 1 No CG composite (Fig. 10a), which has the largest KI among No CG regimes, is still much less saturated near the surface and in the midtroposphere than the Regime 1 FCG composite sounding (Fig. 9a). Comparisons between Figs. 9 and 10 strongly suggest that for all regimes, high lower-tropospheric relative humidity values, relatively steep midtropospheric lapse rates, and a lack of extremely dry air in the midtroposphere are key ingredients for FCG events compared to null events. Finally, there were only minor differences between the composite soundings for the study domain and those for the full peninsula domain (not shown). As examples, composite sounding SBCAPE and PWAT values for most regimes were within 50 J kg^{-1} and 0.3 mm, respectively, when comparing the two domains.

Finally, we highlight the robustness of the NWS TBW partitioning scheme by examining the wind profiles for FCG events (Fig. 9). Results are similar for No CG days (Fig. 10). In Regime 1 (light/variable; Figs. 9a), there are no winds in the surface–400-hPa layer that exceed 2 kt. Regimes 2 and 3 (east-northeast flow; Figs. 9b,c) are similar to each other, but

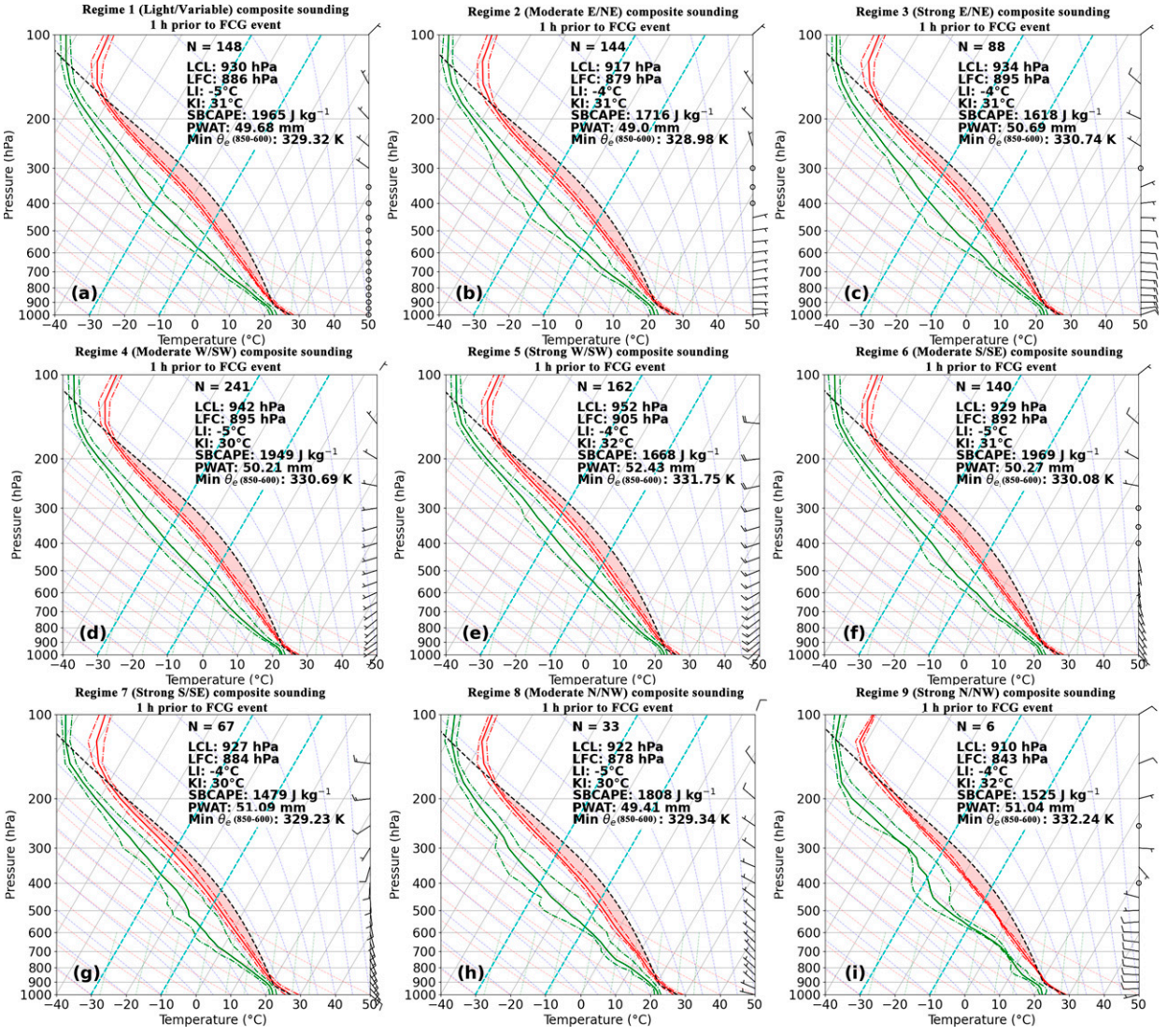

FIG. 9. RAP composite soundings for the nine flow regimes one hour prior (−1 h) to each FCG event, at the RAP grid point closest to each FCG event. Listed on each panel are the number (N) of events in each flow regime and the following composite mean parameters: Lifted condensation level (LCL; hPa), level of free convection (LFC; hPa), lifted index (LI; °C), K index (KI; °C), SBCAPE (J kg^{-1}), PWAT (mm), and minimum θ_e (K) in the 850–600-hPa layer. Unlike in Fig. 4, the SBCAPE area (red shading) and parameters shown on each sounding are calculated by lifting the parcel from the composite mean 1000-hPa temperature (bold solid red line; °C) and dewpoint (bold solid green line; °C). Dashed red and green lines surrounding the environmental temperature and dewpoint represent the interquartile range of the temperature and dewpoint, respectively. Winds (kt; barbs) are plotted on the right-hand side of each panel.

Regime 3 (Fig. 9c) has stronger lower-tropospheric and deeper easterly winds, which help transport moisture from the Atlantic Ocean. Regimes 4 and 5 (Figs. 9d,e) both have deep tropospheric south-southwest flow, but the winds are approximately twice as strong in Regime 5. While Regimes 6 and 7 (Figs. 9f,g) both exhibit surface southeasterly winds, they are twice as strong in Regime 7. In addition, the veering wind profile observed in Regime 7 is considerably weaker in Regime 6. Finally, the N/NW flow is stronger throughout the troposphere in Regime 9 (Fig. 9i) than in Regime 8 (Fig. 9h); we again caution that Regime 9 has only six FCG events.

4. Discussion and conclusions

In this study, we examined the spatiotemporal distributions and convective environments of warm-season (May–September) FCG lightning events for 8 years (2014–21) across the western Florida peninsula and compared them to null (No CG) days. FCG events are identified using NLDN data and subsequently partitioned into nine synoptic-scale flow regimes following the NWS TBW methodology, based on 1000–700-hPa layer-mean vector wind from the 1200 UTC RAP analysis (Fig. 2). Spatiotemporal distributions of FCG events (Figs. 1 and 3; section 3a) show that Regimes 1, 4, and 5 (light/variable,

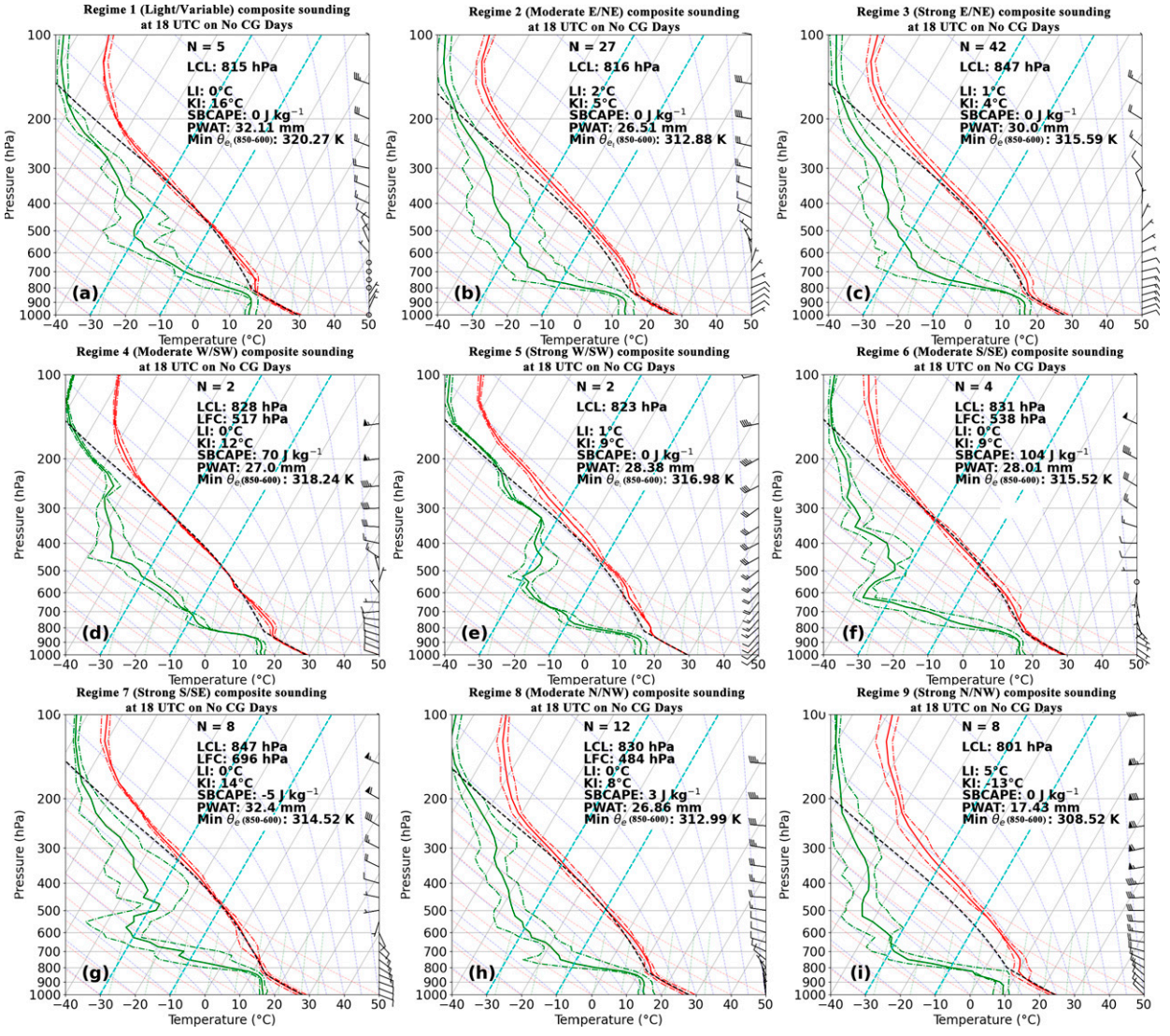

FIG. 10. As in Fig. 9, but at 1800 UTC for No CG days. All soundings were calculated using the area average of a 3 × 3 grid box at the center (27.3°N, 81.975°W) of our study domain (Fig. 1).

moderate W/SW, and strong W/SW flow, respectively) feature the largest number of events, while the fewest events occur in N/NW synoptic-scale flow (Regimes 8 and 9).

The majority of FCG events in Regimes 4 and 5 (W/SW flow) occur in the morning near the Gulf Coast, as the remnant nocturnal land breeze interacts with the west-southwest background flow. Afternoon FCG events in Regimes 4 and 5 occur in the eastern part of the study domain, where the west-southwest flow interacts with the Atlantic sea breeze. For N/NE background flow (Regimes 2 and 3), most FCG events occur in the early afternoon over the eastern part of the study domain, as morning thunderstorms from the eastern Florida peninsula move westward across the state. However, some late-afternoon events occur in southwestern Florida, as the N/NE background flow interacts with the Gulf sea breeze. In S/SE flow (Regimes 6 and 7), most events occur during the early afternoon in the southern half of the domain, as S/SE winds interact with the Gulf sea breeze. FCG events in N/NW flow (Regimes 8 and 9) peak slightly later in the midafternoon and are largely clustered in the southeastern part of the study domain.

We used RAP analysis data to elucidate the environmental characteristics one hour prior to FCG events, as well as at 1200 and 1800 UTC for No CG (null) events. Results (Figs. 4–10; sections 3b and 3c) demonstrate relatively subtle but important differences among the nine FCG event regimes and large differences in all regimes between FCG events and No CG days. Key findings are as follows:

- Among FCG event regimes, Regime 7 (strong S/SE flow) features some of the smallest instability values and weakest midtropospheric lapse rates, but the largest PWAT values of any regime. This regime is characterized by veering winds with height (i.e., warm advection; Fig. 9g) that transport

larger PWAT values from southeast Florida, the Atlantic Ocean, and the Caribbean into the study domain.

- When the synoptic-scale flow comes from the land (i.e., N/NE; S/SE), the "strong" regime (e.g., Regime 3 for N/NE) for each flow direction features larger PWAT than the "moderate" version (e.g., Regime 2 for N/NE). This suggests that stronger background flow is required to transport larger PWAT values from the Atlantic Ocean and/or the Caribbean into the study domain.
- Of the convective parameters examined in this study, SBCAPE (Fig. 4) and PWAT (Fig. 7) exhibit the largest differences among FCG event regimes. However, subtle regime differences and benchmark parameter values (e.g., most FCG events occurring with SBCAPE > 1500 J kg^{-1} and PWAT of 45–55 mm) should also prove useful to regional forecasters.
- Convective parameter differences among the nine FCG event regimes pale in comparison to differences between FCG and No CG days in all regimes. No CG days typically feature little or no SBCAPE, small PWAT values, low near-surface relative humidity values, and weak midtropospheric lapse rates. Comparisons between FCG and No CG days reinforce the vital importance of instability and (especially lower-tropospheric) moisture to warm-season thunderstorms in the Florida peninsula.

Overall, this study provides insight into the spatial and temporal distributions and convective environments of FCG events across the western Florida peninsula that pose a consistent threat to public safety. Future work should include investigating FCG events and No CG days in the eastern Florida peninsula, including the NWS Melbourne and Miami CWAs. A comparison among peninsula and panhandle (e.g., Tallahassee and Jacksonville CWAs) domains would also be fruitful, given the climatological differences in warm-season processes (i.e., two sea breezes in the peninsula versus one in the panhandle). Finally, construction of a FCG environmental composite parameter, along the lines of the supercell composite parameter used operationally by the NWS Storm Prediction Center, may prove useful in improving human forecasts of these events and increasing alert lead times. However, as Doswell and Schultz (2006) detailed, such composite parameters are diagnostics, not forecasts, and should therefore be used cautiously.

To increase the operational relevance of our results, we established a FCG Convective Environment Dashboard (available online at https://www.weather.gov/tbw/TSbrowser) in collaboration with NWS TBW personnel. This enables NWS TBW and other local/regional forecasters to utilize our findings to help increase alert lead times of FCG events. We envision that the Convective Environment Dashboard will consistently evolve, as future research results are incorporated.

Acknowledgments. This research was supported by a University Corporation for Atmospheric Research (UCAR) COMET NWS Partners Project, UCAR Subaward SUBAWD001834. The authors thank Paul Close of NWS TBW for his collaboration on the project and manuscript, as well as Robert Haley of NWS Melbourne for his consultation regarding data availability and webpage construction. We also acknowledge Unidata for supplying a real-time NLDN data feed through the University at Albany, as well as NOAA's National Centers for Environmental Information (NCEI) and Iowa State University's Iowa Environmental Mesonet (IEM) for housing freely available RAP data. Finally, we greatly thank the editor, Roger Edwards of the NWS Storm Prediction Center, and two anonymous reviewers for their helpful comments toward improving this manuscript.

Data availability statement. Real-time NLDN data from Vaisala are available to U.S.-based colleges and universities through the Unidata Local Data Manager (LDM). For information on Unidata's NLDN data distribution, please see https://www.unidata.ucar.edu/data/lightning/nldn.html. Gridded RAP analysis data are freely available from NOAA/NCEI's archive (https://www.ncei.noaa.gov/products/weather-climate-models/rapid-refresh-update) and Iowa State University's IEM (https://mesonet.agron.iastate.edu/archive/). Finally, the analyses and figures resulting from this study are displayed publicly on the NWS TBW CG Convective Environment Dashboard (https://www.weather.gov/tbw/TSbrowser).

REFERENCES

Benjamin, S. G., and Coauthors, 2016: A North American hourly assimilation and model forecast cycle: The Rapid Refresh. *Mon. Wea. Rev.*, **144**, 1669–1694, https://doi.org/10.1175/MWR-D-15-0242.1.

Blair, S. F., D. R. Deroche, J. M. Boustead, J. W. Leighton, B. L. Barjenbruch, and W. P. Gargan, 2011: A radar-based assessment of the detectability of giant hail. *Electron. J. Severe Storms Meteor.*, **6** (7), https://ejssm.com/ojs/index.php/site/article/view/34/34.

Blanchard, D. O., and R. E. Lopez, 1985: Spatial patterns of convection in South Florida. *Mon. Wea. Rev.*, **113**, 1282–1299, https://doi.org/10.1175/1520-0493(1985)113<1282:SPOCIS>2.0.CO;2.

Burrows, W. R., C. Price, and L. J. Wilson, 2005: Warm season lightning probability prediction for Canada and the northern United States. *Wea. Forecasting*, **20**, 971–988, https://doi.org/10.1175/WAF895.1.

Byers, H. R., and H. R. Rodebush, 1948: Causes of thunderstorms of the Florida peninsula. *J. Meteor.*, **5**, 275–280, https://doi.org/10.1175/1520-0469(1948)005<0275:COTOTF>2.0.CO;2.

Courtier, B. M., T. H. M. Stein, R. G. Harrison, K. E. Hanley, and J. M. Wilkinson, 2019: Intensification of single cell storms prior to lightning onset. *Atmos. Sci. Lett.*, **20**, e873, https://doi.org/10.1002/asl.873.

Curran, E. B., R. L. Holle, and R. E. Lopez, 2000: Lightning casualties and damages in the United States from 1959–1994. *J. Climate*, **13**, 3448–3464, https://doi.org/10.1175/1520-0442(2000)013<3448:LCADIT>2.0.CO;2.

Dalu, G. A., and R. A. Pielke, 1989: An analytical study of the sea breeze. *J. Atmos. Sci.*, **46**, 1815–1825, https://doi.org/10.1175/1520-0469(1989)046<1815:AASOTS>2.0.CO;2.

Doswell, C. A., III, and D. M. Schultz, 2006: On the use of indices and parameters in forecasting severe storms. *Electron. J. Severe Storms Meteor.*, **1** (3), https://ejssm.com/ojs/index.php/site/article/view/4/3.

——, H. E. Brooks, and R. A. Maddox, 1996: Flash flood forecasting: An ingredients-based methodology. *Wea. Forecasting*, **11**, 560–581, https://doi.org/10.1175/1520-0434(1996)011<0560:FFFAIB>2.0.CO;2.

Elsenheimer, C. B., and C. M. Gravelle, 2019: Introducing lightning threat messaging using the *GOES-16* day cloud phase distinction RGB composite. *Wea. Forecasting*, **34**, 1587–1600, https://doi.org/10.1175/WAF-D-19-0049.1.

Estoque, M. A., 1962: The sea breeze as a function of the prevailing synoptic situation. *J. Atmos. Sci.*, **19**, 244–250, https://doi.org/10.1175/1520-0469(1962)019<0244:TSBAAF>2.0.CO;2.

Foote, G. B., 1984: A study of hail growth utilizing observed storm conditions. *J. Climate Appl. Meteor.*, **23**, 84–101, https://doi.org/10.1175/1520-0450(1984)023<0084:ASOHGU>2.0.CO;2.

Gentry, R. C., and P. L. Moore, 1954: Relation of local and general wind interaction near the sea coast to time and location of air-mass showers. *J. Atmos. Sci.*, **11**, 507–511, https://doi.org/10.1175/1520-0469(1954)011<0507:ROLAGW>2.0.CO;2.

Gijben, M., 2016: A lightning threat index for South Africa using numerical weather prediction data. M.S. thesis, Dept. of Geography, Geoinformatics and Meterology, University of Pretoria, 145 pp.

Gremillion, M. S., and R. E. Orville, 1999: Thunderstorm characteristics of cloud-to-ground lightning at the Kennedy Space Center, Florida: A study of lightning initiation signatures as indicated by the WSR-88D. *Wea. Forecasting*, **14**, 640–649, https://doi.org/10.1175/1520-0434(1999)014<0640:TCOCTG>2.0.CO;2.

Hansen, A. E., H. E. Fuelberg, and K. E. Pickering, 2010: Vertical distributions of lightning sources and flashes over Kennedy Space Center, Florida. *J. Geophys. Res.*, **115**, D14203, https://doi.org/10.1029/2009JD013143.

Hodanish, S., D. Sharp, W. Collins, C. Paxton, and R. E. Orville, 1997: A 10-yr monthly lightning climatology of Florida: 1986–95. *Wea. Forecasting*, **12**, 439–448, https://doi.org/10.1175/1520-0434(1997)012<0439:AYMLCO>2.0.CO;2.

Holle, R. L., K. L. Cummins, and W. A. Brooks, 2016: Seasonal, monthly, and weekly distributions of NLDN and GLD360 cloud-to-ground lightning. *Mon. Wea. Rev.*, **144**, 2855–2870, https://doi.org/10.1175/MWR-D-16-0051.1.

Johnson, A. W., and K. E. Sugden, 2014: Evaluation of sounding-derived thermodynamic and wind-related parameters associated with large hail events. *Electron. J. Severe Storms Meteor.*, **9** (5), https://ejssm.com/ojs/index.php/site/article/view/57/56.

Kalina, E. A., K. Friedrich, B. C. Motta, W. Deierling, G. T. Stano, and N. N. Rydell, 2016: Colorado plowable hailstorms: Synoptic weather, radar, and lightning characteristics. *Wea. Forecasting*, **31**, 663–693, https://doi.org/10.1175/WAF-D-15-0037.1.

Kingsmill, D. E., 1995: Convection initiation associated with a sea-breeze front, a gust front, and their collision. *Mon. Wea. Rev.*, **123**, 2913–2933, https://doi.org/10.1175/1520-0493(1995)123<2913:CIAWAS>2.0.CO;2.

Knight, C. A., and N. C. Knight, 2001: Hailstorms. *Severe Convective Storms, Meteor. Monogr.*, No. 28, Amer. Meteor. Soc., 223–248.

Koehler, T. L., 2020: Cloud-to-ground lightning flash density and thunderstorm day distributions over the contiguous United States derived from NLDN measurements: 1993–2018. *Mon. Wea. Rev.*, **148**, 313–332, https://doi.org/10.1175/MWR-D-19-0211.1.

Laflin, J., 2013: Verification of RAP model soundings in preconvective environments. *J. Oper. Meteor.*, **1**, 66–70, https://doi.org/10.15191/nwajom.2013.0106.

Lericos, T. P., H. E. Fuelberg, A. I. Watson, and R. L. Holle, 2002: Warm season lightning distribution over the Florida peninsula as related to synoptic patterns. *Wea. Forecasting*, **17**, 83–98, https://doi.org/10.1175/1520-0434(2002)017<0083:WSLDOT>2.0.CO;2.

Livingston, E. S., J. W. Neilsen-Gammon, and R. E. Orville, 1996: A climatology, synoptic assessment, and thermodynamic evaluation for cloud-to-ground lightning in Georgia: A study for the 1996 Summer Olympics. *Bull. Amer. Meteor. Soc.*, **77**, 1483–1496, https://doi.org/10.1175/1520-0477(1996)077<1483:ACSAAT>2.0.CO;2.

López, R. E., and R. L. Holle, 1986: Diurnal and spatial variability of lightning activity in northeastern Colorado and central Florida during the summer. *Mon. Wea. Rev.*, **114**, 1288–1312, https://doi.org/10.1175/1520-0493(1986)114<1288:DASVOL>2.0.CO;2.

Madhulatha, A., M. Rajeevan, M. V. Ratnam, J. Bhate, and C. V. Naidu, 2013: Nowcasting severe convective activity over southeast India using ground-based microwave radiometer observations. *J. Geophys. Res. Atmos.*, **118**, 1–13, https://doi.org/10.1029/2012JD018174.

Mazzetti, T. O., and H. E. Fuelberg, 2017: An analysis of total lightning flash rates over Florida. *J. Geophys. Res. Atmos.*, **122**, 12 812–12 826, https://doi.org/10.1002/2017JD027579.

Medici, G., K. L. Cummins, D. J. Cecil, W. J. Koshak, and S. D. Rudlosky, 2017: The intracloud lightning fraction in the contiguous United States. *Mon. Wea. Rev.*, **145**, 4481–4499, https://doi.org/10.1175/MWR-D-16-0426.1.

Miller, P. W., and T. L. Mote, 2018: Characterizing severe weather potential in synoptically weakly forced thunderstorm environments. *Nat. Hazards Earth Syst. Sci.*, **18**, 1261–1277, https://doi.org/10.5194/nhess-18-1261-2018.

Milrad, S. M., and C. G. Herbster, 2017: Mobile radar as an undergraduate education and research tool: The ERAU C-BREESE field experience with the Doppler on Wheels. *Bull. Amer. Meteor. Soc.*, **98**, 1931–1948, https://doi.org/10.1175/BAMS-D-15-00281.1.

Mosier, R. M., C. Schumacher, R. E. Orville, and L. D. Carey, 2011: Radar nowcasting of cloud-to-ground lightning over Houston, Texas. *Wea. Forecasting*, **26**, 199–212, https://doi.org/10.1175/2010WAF2222431.1.

Murphy, M. J., J. A. Cramer, and R. K. Said, 2021: Recent history of upgrades to the U.S. National Lightning Detection Network. *J. Atmos. Oceanic Technol.*, **38**, 573–585, https://doi.org/10.1175/JTECH-D-19-0215.1.

NOAA, 2021: Historical hurricane tracks. NOAA, accessed 4 January 2022, https://coast.noaa.gov/hurricanes/.

NWS, 2021a: Lightning media. NOAA, accessed 21 June 2021, https://www.weather.gov/safety/lightning-media.

——, 2021b: Florida sea breeze thunderstorm regime methodology. NOAA, accessed 28 June 2021, https://www.weather.gov/tbw/SB_Methodology.

Nicholls, M. E., R. A. Pielke, and W. R. Cotton, 1991: A two-dimensional numerical investigation of the interaction between sea breezes and deep convection over the Florida peninsula. *Mon. Wea. Rev.*, **119**, 298–323, https://doi.org/10.1175/1520-0493(1991)119<0298:ATDNIO>2.0.CO;2.

Orville, R. E., 2008: Development of the National Lightning Detection Network. *Bull. Amer. Meteor. Soc.*, **89**, 180–190, https://doi.org/10.1175/BAMS-89-2-180.

——, and G. R. Huffines, 2001: Cloud-to-ground lightning in the United States: NLDN results in the first decade, 1989–1998. *Mon. Wea. Rev.*, **129**, 1179–1193, https://doi.org/10.1175/1520-0493(2001)129<1179:CTGLIT>2.0.CO;2.

Pielke, R. A., 1974: A three-dimensional numerical model of the sea breezes over South Florida. *Mon. Wea. Rev.*, **102**, 115–139, https://doi.org/10.1175/1520-0493(1974)102<0115:ATDNMO>2.0.CO;2.

Rao, P. A., and H. E. Fuelberg, 2000: An investigation of convection behind the Cape Canaveral sea-breeze front. *Mon. Wea. Rev.*, **128**, 3437–3458, https://doi.org/10.1175/1520-0493(2000)128<3437:AIOCBT>2.0.CO;2.

Rudlosky, S. D., and H. E. Fuelberg, 2011: Seasonal, regional, and storm-scale variability of cloud-to-ground lightning characteristics in Florida. *Mon. Wea. Rev.*, **139**, 1826–1843, https://doi.org/10.1175/2010MWR3585.1.

——, and ——, 2013: Documenting storm severity in the mid-Atlantic region using lightning and radar information. *Mon. Wea. Rev.*, **141**, 3186–3202, https://doi.org/10.1175/MWR-D-12-00287.1.

Schultz, D. M., and P. N. Schumacher, 1999: The use and misuse of conditional symmetric instability. *Mon. Wea. Rev.*, **127**, 2709–2732, https://doi.org/10.1175/1520-0493(1999)127<2709:TUAMOC>2.0.CO;2.

Schwartz, B. E., and L. F. Bosart, 1979: The diurnal variability of Florida rainfall. *Mon. Wea. Rev.*, **107**, 1535–1545, https://doi.org/10.1175/1520-0493(1979)107<1535:TDVOFR>2.0.CO;2.

Shafer, P. E., and H. E. Fuelberg, 2006: A statistical procedure to forecast warm season lightning over portions of the Florida peninsula. *Wea. Forecasting*, **21**, 851–868, https://doi.org/10.1175/WAF954.1.

——, and ——, 2008: A perfect prognosis scheme for forecasting warm-season lightning over Florida. *Mon. Wea. Rev.*, **136**, 1817–1846, https://doi.org/10.1175/2007MWR2222.1.

Statista, 2021a: Population of the Tampa-St. Petersburg-Clearwater metro area in the United States from 2010 to 2020. Accessed 29 December 2021, https://www.statista.com/statistics/815278/tampa-metro-area-population/.

——, 2021b: Population of the Orlando-Kissimmee-Sanford metro area in the United States from 2010 to 2020. Accessed 29 December 2021, https://www.statista.com/statistics/815299/orlando-metro-area-population/.

Williams, E., and Coauthors, 1999: The behavior of total lightning activity in severe Florida thunderstorms. *Atmos. Res.*, **51**, 245–265, https://doi.org/10.1016/S0169-8095(99)00011-3.

——, V. Mushtak, D. Rosenfeld, S. Goodman, and D. Boccippio, 2005: Thermodynamic conditions favorable to superlative thunderstorm updraft, mixed phase microphysics and lightning flash rate. *Atmos. Res.*, **76**, 288–306, https://doi.org/10.1016/j.atmosres.2004.11.009.